scientific reports

Check for updates

OPEN

Preclinical approach of two novel tetrahydroquinoline derivatives targeting GPER and Bcl-2 for anti-glioblastoma therapy

David Méndez-Luna[1,2], Loreley-Araceli Morelos-Garnica[1], José-Rubén García-Sánchez[3], Gilles Joucla[4], Laurent Bonneau[4], Norbert Bakalara[4]✉ & José Correa-Basurto[1]✉

Glioblastoma multiforme (GBM), is a rapidly growing and aggressive brain tumor that can arise *de novo* in the brain or evolve from lower-grade astrocytoma. This malignancy represents a medical challenge due to the tumor´s localization in the brain, high rates of Temozolomide (TMZ) resistance, and extensive malignant cell parenchymal infiltration, among other factors. Consequently, new drug discovery efforts have focused on targeting pivotal pharmacological targets such as GPER and Bcl-2, presenting a promising strategy for developing new GBM treatments. Herein, we present the results of an improved structure guided design of anti-glioblastoma compounds, L-06 and L-37, both containing the tetrahydroquinoline scaffold and a sulfonamide moiety recognized by GPER and Bcl-2 binding sites, respectively. Both compounds were evaluated in a battery of in vitro assays to measure their anti-glioblastoma activity. L-06 and L-37 were subjected to chemical stability testing under forced degradation conditions indicated minimal degradation from 0.15 to 13.6%. Additionally, antiproliferative evaluation in 2D cell culture yielded IC_{50} values between 39 and 67 µM in GBM cell lines LN18 and U373, consistent with Gossypol, a well-known Bcl-2 inhibitor. G-15 and L-37 to a greater extent than L-06, inhibit neurospheres formation in glioblastoma stem cells (Gli4) cultured in a proliferation medium. Moreover, in 3D antiproliferative assays using glioblastoma stem cells on non-aligned nanofibers L-37 showed better inhibitory effect than L-06. Interestingly, L-06 than L-37 exhibited an antimigratory effect on glioblastoma stem cells loaded onto aligned nanofibers at concentrations where no antiproliferative activity were observed, unlike G-15, a poorly water soluble GPER antagonist. Collectively, these findings establish a preclinical foundation for L-37 and L-06 as potential anti-glioblastoma agents and support their further investigation as therapeutic candidates.

GBM, a grade IV astrocytoma, is the most common malignant and deadly primary brain tumor according to the World Health Organization (WHO), accounting for ~60% of total brain tumor in adults, with a global incidence of <10 *per* 100,000 individuals and 5.9 individuals just for North America[1,2]. The standard of care (SoC) involves a multimodal approach, including surgery, radiation, and chemotherapy employing TMZ[3–5] reaching a median survival of ~15 months[6–8]. However, tumor progression and recurrence are inevitable because malignant cells develop TMZ and radiotherapy resistance and cancer cells invade parenchyma limiting the therapeutic options for patients[9–13]. Due to GBM is a highly heterogeneous neoplasm, a large-scale analysis of genetic aberrations occurring in tumor cells identified three main signaling pathways deregulated: activation of the receptor tyrosine kinase (RTK)/Ras/phosphoinositide 3-kinase (PI3K) pathway (~88%), inhibition of p53 (~87%), and retinoblastoma protein (Rb) signaling pathways (~78%), delimiting the strategies for drug targeting on many of these commonly observed alterations[14,15]. Regarding kinase pathways, recent data points to activation of c-Met in GBM leading to an increased levels of the anti-apoptotic Bcl-2 family members[16]. Indeed,

[1]Laboratorio de Diseño y Desarrollo de Nuevos Fármacos e Innovación Biotecnológica, Escuela Superior de Medicina, Instituto Politécnico Nacional, Plan de San Luis y Díaz Mirón s/n, Col. Casco de Santo Tomas, Alcaldía Miguel Hidalgo, Mexico City C.P. 11340, México. [2]Departamento de Fisiología, Escuela Nacional de Ciencias Biológicas, Instituto Politécnico Nacional. Zacatenco, Av. Wilfrido Massieu 399, Col. Nueva Industrial Vallejo, Alcaldía Gustavo A. Madero, Ciudad de México C.P. 07738, México. [3]Laboratorio de Oncología Molecular y Estrés Oxidativo de la Escuela Superior de Medicina, Instituto Politécnico Nacional, Plan de San Luis y Díaz Mirón, s/n, Col. Casco de Santo Tomas, Ciudad de México 11340, Mexico. [4]Univ. Bordeaux, CNRS, Bordeaux INP, CBMN, UMR 5248, Pessac F-33600, France. ✉email: Norbert.Bakalara@enstbb.fr; corrjose@gmail.com

Bcl-2, Bcl-xL and Mcl-1 have arisen as viable targets for glioblastoma treatment according to the up-regulated expression analyzed in these tumors[17]. Specifically, the Bcl-2 protein has been interesting as a biological target due to their BH3 domain, which is an orchestrator into the suppression of its activity and expression[18]. In the same way, estrogen activity has been analyzed in GBM tumor cells, defining aromatase and classic estrogen receptors α and β (ERα and ERβ) expression, in addition to local estrogen production which promotes tumor growth[19,20]. Besides, fast, or non-genomic effects of estrogens have been studied in GBM, attributed this estrogen rapid-signaling to a transmembrane G-protein coupled estrogen receptor (GPER). In this context, epidermal growth factor receptor (EGFR), triggering the mitogen-activated protein kinase/extracellular signal-regulated kinase pathway and, activation of the phospholipase C (PLC) and phosphatidylinositol 3-kinase (PI3K) pathways, promoting the transcription of genes related to cell survival, proliferation, and apoptosis, have been demonstrated being triggered by the activation of GPER in several cell models[21–23]. Taken together, the recent data about promissory pharmacological targets for GMB therapy, points to the feasibility of apply the multitarget inhibition as a strategy to face-off this disease, indicating that simultaneous modulation of multiple targets may improve both therapeutic safety and efficacy, compared with single-target drugs, leading to a better prognosis and an increase in survival of the individuals affected by this disease[24,25]. Indeed, the dual-inhibition approach targeting the aberrant activity of GPER and Bcl-2 becomes evident when analyzing the crosstalk between these pharmacological targets. Inhibition of GPER downregulates the GPER/ERK signaling pathway, which promotes cell growth and survival by increasing Bcl-2 levels, with EGFR activity acting as the primary orchestrator. Consequently, the inhibition of GPER activity is likely to lead to EGFR inactivation, resulting in a reduction of Bcl-2 anti-apoptotic activity, presumably due to a negative feedback mechanism. This multitarget approach offers several advantages, including the mitigation of clonal heterogeneity, a reduced risk of multi-drug resistance (MDR), decreased drug toxicity due to the use of more than one drug, and, ultimately, fewer side effects[26,27]. In this way, our research group, applying a protocol of computational rational design of multi-target new drugs, we selected as the most promising two compounds targeting the binding sites on GPER and Bcl-2[28]. Thus, herein we show the results of an improved chemical synthesis, and the preclinical evaluation on a cluster of GBM cancer cells including functional 2D and 3D cell cultures and anti-migratory assays, of the compounds named L-06 and L-37. Remarkably, both compounds depicted better performance (IC_{50} values) on the assayed cell lines than Gossypol (Bcl-2 inhibitor), and G-15 (GPER antagonist). Besides, it is worth noting that LN18 and U373 cell lines expressing GPER were more sensitive to L-37 than L-06, moreover, such compound interestingly showed a lesser cytotoxic effect on BJ cell line (non-transformed cell line). Furthermore, G-15 and L-37 to a greater extent than L-06, inhibit neurospheres formation in glioblastoma stem cells (Gli4) cultured in a proliferation medium. Besides, in 3D antiproliferative assays using glioblastoma stem cells on non-aligned nanofibers, cultured in differentiation medium, L-37 demonstrated a better performance measured as antiproliferative effect than L-06. Strikingly, L-06 than L-37 exhibited a better antimigratory effect on glioblastoma stem cells loaded onto aligned nanofibers at concentrations where no antiproliferative activity was observed, unlike to G-15, a poorly water soluble GPER antagonist. Altogether, these findings denote the safety and potential druggability of L-37 and L-06 as agents against GBM disease.

Materials and methods

Chemical synthesis and characterization

An improved synthetic procedure based on the reaction conditions established by Morelos-Garnica et al.[28], was developed to increase the yield and avoid the formation of additional byproducts (Fig. 1). Reagent-grade chemicals were sourced from commercial suppliers and employed without additional purification. The reaction progress was followed using thin-layer chromatography (TLC) on aluminum-backed sheets coated with silica gel 60 GF254 (HX805651) and a fluorescent indicator, visualizing them under UV light at 254 nm. Melting points (mp) were determined on an Electrothermal IA 91,000 apparatus (Electrothermal, Bibby Scientific, Staffordshire, ST15 OSA, UK). ^{1}H and ^{13}C NMR spectra were acquired employing deuterated chloroform ($CDCl_3$) as the solvent and tetramethylsilane (TMS) as the internal reference on a Varian Mercury 300 MHz spectrometer and a Bruker Avance III 750 MHz spectrometer, respectively. Chemical shifts (δ) are denoted in ppm relative to the TMS standard, while coupling constants are expressed in Hertz (Hz). Agilent 6545 QTOF LC/MS equipment (Agilent Technologies, Santa Clara, CA, USA) was used for electrospray ionization mass spectrometry MS/MS in positive mode (ESI-MS/MS).

Synthesis of (3aS,4R,9bR)-4-(6-bromobenzo[d][1,3]dioxol-5-yl)-N-tosyl-3a,4,5,9b-tetrahydro-3 H-cyclopenta[c] quinoline-8-carboxamide (L-06)

Briefly, for L-06 compound, to a well-stirred solution of *p*-toluenesulfonamide (173 mg, 1.01 mmol, 1.2 eq) in dimethylformamide (DMF) (2 mL) was added (3aS,4R,9bR)-4-(6-bromobenzo[d][1,3]dioxol-5-yl)3a,4,5,9b-tetrahydro-3H-cyclopenta[c] quinoline-8-carboxylic acid (named inhouse G1-PABA) (350 mg, 0.84 mmol, 1.0 eq), N-(3-dimethylaminopropyl)-N′-ethylcarbodiimide hydrochloride (EDC·HCl) (162 mg, 0.84 mmol, 1.0 eq), hydroxybenzotriazole (HOBt) (11.4 mg, 0.08 mmol, 0.1 eq), and 4-dimethylaminopyridine (DMAP) (103 mg, 0.84 mmol, 1.0 eq) previously dissolved in DMF, giving a final volume of 10 mL. The reaction was stirred at 45°C for 72 h. The process of the reaction was tracked using TLC with silica gel 60 (230–400 mesh). After the reaction elapsed, this was extracted with Ethyl acetate (EtOAc) and washed with distilled H_2O (3 X), and a last wash with a saturated $NaHCO_3$ solution. The combined organic extracts were dried over anhydrous Na_2SO_4, filtered, and concentrated under reduced pressure. The crude reaction was purified using a mixture of hexane/EtOAc (4:6) as the eluent, affording 45% yield of compound as a yellow syrup. Rf = 0.52 (Hexane/EtOAc, 5:5), mp = 171.3°C (Not corroborated). The high-pressure liquid chromatography (HPLC) Uv/Vis purity obtained was 95.63%. ESI-MS (MS/MS) value for $C_{27}H_{23}BrN_2O_5S$ [M + H] calculated = 566.0511; found = 566.0491. IR (KBr) Vmax: 3313, 2922, 1655, 1602, 1471, 1223, 1033, 659 cm^{-1}. ^{1}H NMR (750 MHz, $CDCl_3$) δ 7.28 (s, H-7′),

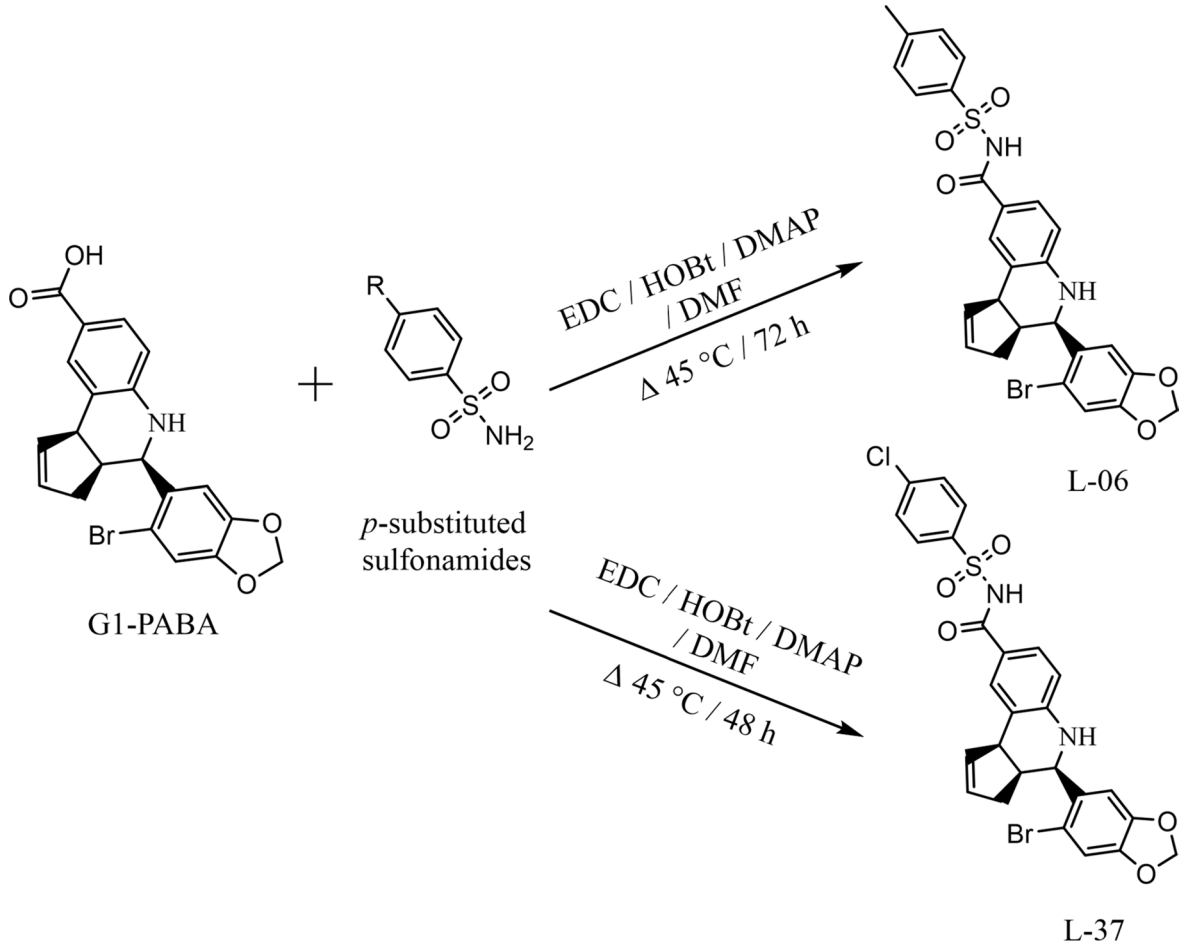

Fig. 1. Synthetic procedure of L-06 and L-37. Reactants and chemical synthesis conditions are listed up – down from the arrows for each compound, as appropriate. For L-06 was employed p-toluenesulfonamide and, for L-37 was employed 4-chlorobenzenesulfonamide, as *p*-substituted sulfonamides.

δ 7.18 (s, H-9), δ 7.13 (s, H-4'), δ 7.08 (dd, J = 8.2, 1.5 Hz), δ 7.00 (d, J = 2.3 Hz, H-7), δ 6.59 (d, J = 8.2 Hz, H-6), δ 5.99–5.98 (d, J = 9.7 Hz, H2'), δ 5.84 (dd, J = 2.7, 1.4 Hz, H-1), δ 5.65 (d, J = 4.8 Hz, H-2), δ 4.89 (D, J = 3.2 Hz, H-4), δ 4.11 (d, J = 7.2 Hz, H-9b), δ 3.18 (dd, J = 9.2 Hz, 5.2 Hz, H-3a), δ 2.62 (CH_3), δ 1.80 (dd, J = 15.8 Hz, 9.0 Hz, H-3). ^{13}C NMR (189 MHz, $CDCl_3$), δ 171.93 (CO), δ 147.58 (C-7'a), δ 147.38 (C-3'a), δ 146.00 (C-5'), δ 134.13 (C-8), δ 133.86 (C-9b, C1"), δ 130.41 (C-2), δ 129.05 (C-7), δ 126.53 (C-5", C-3"), δ 126.04 (C-2", C-6"), δ 125.55 (C-6', C-4"), δ 115.30 (C-6), δ 113.05 (C-1), δ 112.91 (C-7'), δ 107.97 (C-4'), δ 101.82 (C-2'), δ 56.52 (C-4), δ 45.80 (C-9b), δ 42.10 (C-3a), δ 31.42 (C-3), δ 21.04 (CH_3).

Synthesis of (3aS,4R,9bR)-4-(6-bromobenzo[d][1,3]dioxol-5-yl)-N-((4-chlorophenyl) sulfonyl)-3a,4,5,9b-tetrahydro-3 H-cyclopenta[c] quinoline-8-carboxamide (L-37)

For L-37 compound, to a well-stirred solution of 4-chlorobenzenesulfonamide (100 mg, 0.52 mmol, 1.0 eq) in DMF (2 mL), was added G1-PABA (259 mg, 0.62 mmol, 1.0 eq), EDC·HCl (99.8 mg, 0.52 mmol, 1.0 eq), HOBt (7 mg, 0.05 mmol, 0.1 eq), and DMAP (63 mg, 0.52 mmol, 1.0 eq) previously dissolved in DMF, giving a final volume of 10 mL. The reaction was stirred at 45°C for 48 h. The process of the reaction was tracked using TLC with silica gel 60 (230–400 mesh). After completion of the reaction, the reaction mixture was extracted with EtOAc and washed with H_2O (3 X) and a last wash with a saturated $NaHCO_3$ solution. The combined organic extracts were dried over anhydrous Na_2SO_4, filtered, and concentrated under reduced pressure. The crude reaction was purified by flash chromatography silica gel 60 (230–400 mesh), using a mixture of Hexane/EtOAc (4:6) as the eluent, affording 40% yield of compound as a white powder. Rf = 0.50 (Hexane/EtOAc, 5:5), mp = 160.7°C (Not corroborated). The HPLC Uv/Vis purity obtained was 95.30%. ESI-MS (MS/MS) value for $C_{26}H_{20}BrClN_2O_5S$ [M + H] calculated = 585.9965; found = 585.9948. IR (KBr) Vmax: 3350, 2914, 1685, 1608, 1479, 1233, 114, 1037, 831, 704 cm^{-1}. ^{1}H NMR (750 MHz, $CDCl_3$) δ 7.28 (s, H-7'), δ 7.19 (s, H-9), δ 7.13 (s, H-4'), δ 7.08 (dd, J = 8.2, 1.9 Hz, H-2", H-3", H-5", H-6"), δ 7.03 (d, J = 2.3 Hz, H-7), δ 6.59 (d, J = 8.2 Hz, H-6), δ 5.99–5.98 (d, J = 9.8 Hz, H2'), δ 5.85 (dd, J = 2.8, 1.4 Hz, H-1), δ 5.65 (d, J = 4.6 Hz, H-2), δ 4.90 (d, J = 3.3 Hz, H-4), δ 4.10 (d, J = 8.6 Hz, H-9b), δ 3.18 (dd, J = 9.0 Hz, 3.3 Hz, H-3a), δ 1.80 (dd, J = 15.6 Hz, 8.9 Hz, H-3). ^{13}C NMR (189 MHz, $CDCl_3$), δ 171.93 (CO), δ 147.58 (C-7'a), δ 147.38 (C-3'a), δ 146.94 (C-5'), δ 134.13 (C-8), δ 133.86 (C-9b, C1"), δ 130.42 (C-2), δ 129.05 (C-7), δ 126.57 (C-5", C-3"), δ 126.05 (C-2", C-6"), δ 125.57 (C-6',

	Mobile Phase	
Time (min)	A (water) %	B (MeCN) %
0	40	60
8	10	90
10	10	90
15	40	60

Table 1. Mobile phase proportions of the purity analysis methodology.

Type of condition	Acid	Basic	Oxidative	Luminous	Thermal
Medium conditions	HCl 0.1 N	NaOH 0.1 N	H_2O_2 3%	Sunlight	50 °C
Time of exposition	24 h	24 h	1 h	24 h	24 h

Table 2. Forced stress conditions.

C-4"), δ 115.29 (C-6), δ 113.06 (C-1), δ 112.92 (C-7'), δ 107.97 (C-4'), δ 101.82 (C-2'), δ 56.53 (C-4), δ 45.80 (C-9b), δ 42.10 (C-3a), δ 31.43 (C-3).

Purity analysis by HPLC-Uv/vis

The HPLC purity analysis was performed using an Agilent 1260 infinity series liquid chromatograph (Agilent Technologies, Palo Alto, CA, USA) equipped with a quaternary pump delivery system (G1311B), robotic autosampler (G1316A), column thermostat (G1316A) and multi wavelength UV detector (G1315C), the results were analyzed in OpenLab CDS EZChrom. The employed mobile phase consisted in a gradient of (A) water and (B) acetonitrile (MeCN), and the proportions are shown in Table 1. Every day, the mobile phase was freshly prepared utilizing deionized water that had been filtered through a 0.22 µm filter and degassed before use. The flow rate was set at 0.8 mL/min. The procedure employed a Zorbax Eclipse XDB-C18 column (5 m, 4.6 × 150 mm) and was conducted 25 °C. Acceptable purity for all compounds was set as a value upper at 95%.

Forced stability test

Synthesized compounds were submitted to a chemical forced stability test to corroborate protecting patient safety and validating chemical stability[29]. Briefly, the stock solution of the compound was of 600 µm/mL, and an aliquot of 1 mL was taken and placed on an individual volumetric flask of 5 mL for each forced stress condition. For the acid and basic condition, 1 mL of the HCl 0.1 N or NaOH 0.1 N solution were added to the respective volumetric flask that already contains 1 mL of the stock solution, allowing to settle for 24 h, then the reactions were neutralized with 1 mL of NaOH 0.1 N for the case of the acid condition and with 1 mL of HCl 0.1 N for the case of the basic condition. Finally, they were brought to volume with mobile phase (MeCN: Water 60:40 v/v), to 120 µg/mL. For the oxidative condition, 1 mL of H_2O_2 3% solution was placed in the volumetric flask already containing 1 mL of stock solution, settled for 1 h and after the exposure time, brought to volume with mobile phase (MeCN: Water 60:40 v/v), to 120 µg/mL. For the thermal condition, 1 mL of the stock solution was brought to volume with mobile phase, placed in a vial with a lid to prevent evaporation of the mobile phase solvents, and placed in a lab drying oven at 50 °C for 24 h. Lastly, for the light condition, 1 mL of the stock solution was brought to volume with mobile phase, placed in a vial with a lid, and exposed to sunlight for 24 h. All solutions were prepared by triplicate, each condition had a blank to rule out peaks related to the mobile phase and solutions added. The specific conditions of each environmental stress condition are collected in Table 2.

Cell culture

Anti glioblastoma activity of the synthesized compounds was assayed on two GBM cell lines (LN-18 and U373) and the glioblastoma stem cell Gli4, which express several typical markers of neural precursors which are part of a multicomponent with potential to generate tumors in vivo[30]. In detail, LN-18 (ATCC, CRL-2610, Rockville, MD, USA) and U-373 were grown in Dulbecco's Modified Eagle medium (DMEM, (Life Technologies, Gaithersburg, MD, USA) phenol-red free, and 1% of streptomycin/penicillin (Gibco), supplemented with amino acids and Fetal Bovine Serum (FBS) 5%, at 37 °C and 5% of CO_2. For neurospheres formation, Gli4 glioblastoma stem cells were cultured in proliferation media on low attachment microplates according to the protocol described elsewhere[30]. Briefly, proliferation medium (DMEM/F12 medium supplemented with glucose, glutamine, insulin, N2, Epidermal Growth Factor and Fibroblast Growth Factor). Moreover, for 3D antiproliferative and antimigratory assays, Gli4 cells were cultivated in proliferation and differentiation medium (DMEM/F12 medium supplemented with the same components as for the proliferation medium except the growth factors and heparin replaced by Fetal Bovine Serum (0.5%)). Non-aligned nanofibers were used for antiproliferative assays, while aligned nanofibers were used for antimigratory assays. Moreover, as control cell lines, the human fibroblast cells BJ (ATCC, CRL-2522) and breast epithelial cells MCF-10 A (ATCC, CRL-10317) cell lines were used. BJ cells were grown in DMEM medium, 100 U/mL penicillin, 100 mg/mL streptomycin and FBS 5% at 37 °C and 5% of CO_2. MCF10A cells were grown in DMEM/F12 medium supplemented with 100 U/mL penicillin,

100 mg/mL streptomycin, horse serum (5%), insulin, Epidermal Growth Factor (EGF), and hydrocortisone at 37 °C and 5% of CO_2.

Antiproliferative assay based on 2D cell culture

The anti-glioblastoma activity of the synthesized compounds on 2D cell cultures was carried out with an MTT [3-(4,5-Dimethylthiazol-2-yl)-2,5-diphenyltetrazolium Bromide] assay. Thus, for LN-18, U373, as well as on BJ and MCF-10 A when cells reach confluence, a density of 1×10^3 cells were seeded in 96-well plates, and after 24 h to allow adherence to the plate, cells were exposed to 0 µM to 140 µM of the tested compounds and control drugs (Gossypol, a Bcl-2 inhibitor) using DMSO 0.1% as vehicle control. Time exposure was set at 24 h (data not shown) or 48 h. The assay was conducted by adding 100 µL of MTT (Sigma, St Louis, MO, USA) (2.5 mg/mL in clear medium without phenol red) to each well, and incubating for 1 h at 37 °C, 5% CO_2. Once the time concluded, the medium of each well was replaced by 200 µL of DMSO (reagent grade). Subsequently, absorbance, which acts as an indicator of cellular metabolic activity was measured at 540 nm in a Mark™ Microplate Absorbance Reader (Bio-Rad Laboratories, Hercules, CA, USA). One-way ANOVA was used to determine statistical significance ($P \leq 0.05$) between each treatment and the DMSO control. Group means were compared using Tukey's post hoc comparison if significant. P-values were used to establish statistical significance, with $p > 0.05$ indicating statistical significance. Plots were built with GraphPad Prism 8.0 through a logarithmic analysis of variable scope. A two-way ANOVA was used to determine statistical significance ($P \leq 0.05$) between treatments. Group means were compared using Tukey's post hoc comparison if significant. P-values were used to establish statistical significance, with $p > 0.05$ indicating statistical significance. Concerning Gli4 cells, a density of 4×10^3 were dissociated and transferred in each well of a 96-well plate pre-coated with poly-2-hydroxyethyl methacrylate. Follow the addition of the corresponding volume of the stock solutions of L-06, L-37 and G15 in DMSO to obtain a final concentration of 0, 1 and 10 µM. The plates were incubated for 4 days and when the time elapsed the cells were dissociated and counted. The cell counting was performed with a Neubauer chamber taking an aliquot of 10 µL of each well plus 10 µL of Trypan blue as dye.

Neurospheres formation assays

Regarding Gli4 cells for neurospheres (NS) formation, we replicated the method described by our research group and published elsewhere[31]. Briefly, a density of 4×10^3 cells were dissociated and transferred in each well of a 96-well plate round-bottom ultra-low attachment microplate coated with a covalently non-bonded hydrogel (Corning 7007) pre-coated with poly-2-hydroxyethyl methacrylate. Follow the addition of the corresponding volume of the stock solutions of L-06, L-37 and G15 in DMSO to obtain a final concentration of 0, 1 and 10 µM. The plates were incubated for 4 days and when the time elapsed the cells were dissociated and counted. The cell counting was performed with a Neubauer chamber taking an aliquot of 10 µL of each well plus 10 µL of Trypan blue as dye.

3D nanofiber matrix

Polyacrylonitrile nanofibers (NFS) were produced by electrospinning in either a non-aligned or aligned pattern, as described previously[31]. The NFSs were cut into pieces and sterilized using standard autoclave procedures before their biological application. For further information about NS scaffold synthesis see Supplementary Material.

Antiproliferative assay based on 3D cell culture models

The 3D antiproliferative assay consisted of neurospheres (NS) loaded and placed on non-aligned NFS to analyze the compound's effect on a tumor-like environment. In detail, Gli4 cells were first cultured in a proliferation medium to form NS in anti-adherent flasks then were dissociated in Hanks' Balanced Salt Solution (HBSS) and seeded into a 96-well microplate containing pieces of non-aligned NFSs at a density of 4×10^3 cells in 20 µL *per* well. Drugs were added along with either proliferation or differentiation medium, bringing the total volume to 200 µL *per* well. Cells were cultured for 4 days in differentiation medium, subsequently, an MTT assay was performed as described below. The culture medium was discarded and replaced with 90 µL of medium containing 10 µL of MTT solution (5 mg/mL in Phosphate-buffered saline (PBS)). The plate was incubated for 4 h in a CO_2 incubator. After incubation, the supernatant was discarded and replaced with 100 µL of DMSO, followed by vigorous shaking for 2 h at room temperature (rt) to dissolve the formazan crystals. The entire volume was then transferred to a new microplate for absorbance measurement at 570 nm. A blank control was prepared using NFSs incubated in DMSO.

3D anti-migratory assay

Gli4 cells were cultured in proliferation medium to form NS in an anti-adherent round-bottom 96-well microplate until the NS reached a diameter of 500 µm. The NS were then transferred with a 20 µL micropipette onto the center of disc-shaped patches of aligned NFS in flat-bottom 96-well microplate. After a 30-minute incubation, wells were filled with 200 µL of differentiation medium containing different concentrations of drugs. The NS were incubated for 6 days before performing fluorescence microscopy analysis. Fixation, permeabilization, washing, and staining of cells from 3D anti-migratory assay were performed directly in the microplate. First, the culture supernatant was discarded, and the fiber disc patches were washed twice with PBS at 37 °C. Next, 100 µL of 4% formaldehyde in PBS was added as a fixative. After 15 min of shaking at rt, the fiber disc patches were washed 3 X for 5 min each in PBS. Cells were permeabilized by adding 100 µL of a solution containing 5% FBS and 0.5% Triton X-100 in PBS. After 30 min of shaking at rt, the fiber disc patches were washed 3 X for 5 min each in PBS. Cells were then stained by adding 100 µL of ReadyProbes 488, which targets actin. After 30 min of incubation at rt, the fibre disc patches were washed 3 X for 5 min each in PBS. The fibre patches were mounted on

glass slides and covered with Fluoromount mounting solution and cover slide. Cells were observed using a Zeiss Axio-Observer 7 inverted microscope (Colibri 7 lamp, AxioCam 705 Mono camera), and images were analyzed using the Zen Analysis module. Statistical analysis: Migration Surface: Non-parametric Mann-Whitney test - % Viability: p-values from one-way repeated ANOVA - $n=3$ * $p<0.05$ ** $p<0.005$. For further information about Flow Cytometry see Supplementary Material.

Western blot analysis

Analysis of the GPER expression was corroborated through western blot. Hence, cells grown in culture were subjected to homogenization using RIPA (Radioimmunoprecipitation assay) buffer and protease inhibitors. Protein concentration was measured using a Bradford protein assay. Electrophoresis of proteins was conducted as follows: the protein extract was heated for 5 min, subsequently, protein samples containing 100 µg of total crude protein underwent electrophoresis using a 12% SDS-polyacrylamide gel. The resulting gel was then transferred onto a nitrocellulose membrane. A solution of 5% nonfat dry milk in Tris-buffered saline was used to block the membranes to avoid the noise presence. Afterwards, the primary antibody was incubated overnight with the appropriate dilutions, being the antibody used for GPER (Antibodies, A12843). Following treatment, the membranes were washed with Tris-buffered saline (3X) before being incubated for 1 h at rt with a secondary antibody, specifically the horseradish peroxidase-conjugated anti-rabbit IgG secondary antibody proper for GPER expression.

Results and discussion

L-06 compound shows enantiomeric excess by HPLC UV/Vis

Chemical purity is essential for developing safe medicines and for conducting research to obtain reliable results, while also adhering to the guidelines of the International Council for Harmonization. In this context, one of the most used methods to identify substances and ensure their purity is the HPLC, which allows impurity quantity detection and pharmaceutical formula clarification. Thus, once obtained the chromatograms corresponding to the purity analysis of the synthesized compounds (Fig. 2), the yielded results for L-06 compound gave two peaks (Fig. 2A), peak 1 with a Retention Time (RT) of 5.76 min and peak 2 with a RT of 7.84 min, which were subsequently separated employing a fraction collector coupled to the HPLC, and then analyzed with the mass spectrometer to determine the molecular mass of both peaks. Interestingly, both peaks showed the same observed mass and isotopic distribution pattern corresponding to a compound with a bromine atom in their structure (Fig. 3A - B). Therefore, the result yielded by the purity analysis showed the presence of enantiomeric excess for L-06 compound may be due to an electronic rearrangement that has direct influence in the stereo genic center corresponding to the benzylic proton of the piperidine ring triggering the presence of two probable enantiomers without being able in this work to delimit the type of enantiomer that each peak corresponds. Whilst, for L-37 the purity analysis was able to detect only a peak for the compound (Fig. 2B), denoting the stability that the chlorine atom confers to the structure avoiding the probable electronic rearrangement that L-06 presents. Nevertheless, further improvement in the chemical synthesis of both analyzed compounds is further required, with particular emphasis on L-06, to achieve complete structural elucidation using more sophisticated methods. These methods may include chiral gas chromatography (GC), primarily performed on chiral stationary phases (CSPs), or supercritical fluid extraction (SFE), which utilizes solvents at conditions above both the critical temperature and pressure to conduct finally, X-ray diffraction. Notably, SFE has previously been used to separate the enantiomers of 6-Fluoro-2-methyl-1,2,3,4-tetrahydroquinoline (FTHQ)[32], a compound with structural similarities to those analyzed in this study.

L-06 and L-37 are safe compounds with neglectable values of degradation

Forced stress tests are a critical part of the drug development process, which provides insight into the inherent stability of synthesized compounds with high druggability properties to the development and validation of stability-indicating analytical methods. In this sense, chromatograms yielded by HPLC Uv-vis corresponding to each condition assayed for L-06 (Fig. 4) as part of the forced stress assay, depicts that L-06 is slightly more sensitive for acid and basic conditions (7.2% and 9.8% of degradation, respectively) than the others assayed. Furthermore, L-37 was the less sensitive compound for most of the conditions assayed, with only a special sensitivity for basic and luminous conditions depicting a 13.6% and 3.5% of degradation, respectively (Fig. 5). Notably, although the degradation values of both compounds indicate suitable chemical stability, further research is required to identify optimal pharmaceutical vehicles or nanocarriers that ensure effective drug delivery to the central nervous system (CNS). This research should focus on conditions inherent to the human body, such as plasma pH, the blood-brain barrier (BBB), and plasma-protein interactions, which can hinder the achievement of accurate drug concentrations at the target site. In this regard, our research group is currently using PAMAM dendrimers (promising nanocarriers that have been detected elsewhere in the brain under ischemic conditions 24 h after administration[33]) demonstrating their potential as delivery vectors for therapeutic applications in glioblastoma (GBM) treatment[29–34]. All the percentage degradation values obtained in each assayed condition for both compounds are collected in Table 3.

L-06 and L-37 are potential anti glioblastoma compounds by 2D cell-based evaluations

Synthesized compounds were subjected to an anti-proliferative evaluation in 2D cell cultures to analyze their potential anti glioblastoma activity in two different cancer cell lines characterized by an overexpression of Bcl-2 protein[35,36]. Detailing, the compounds were tested on two human cancerous cell lines of GBM, LN-18 and U373 yielding promising IC_{50} values by conducting an MTT assay (IC_{50} values are collected in Table 4). In addition, when compared to the reference compounds (Gossypol, a naturally occurring polyphenolic compound identified as a small-molecule inhibitor of the anti-apoptotic Bcl-2 protein, and G15, a GPER antagonist with selective activity

A)

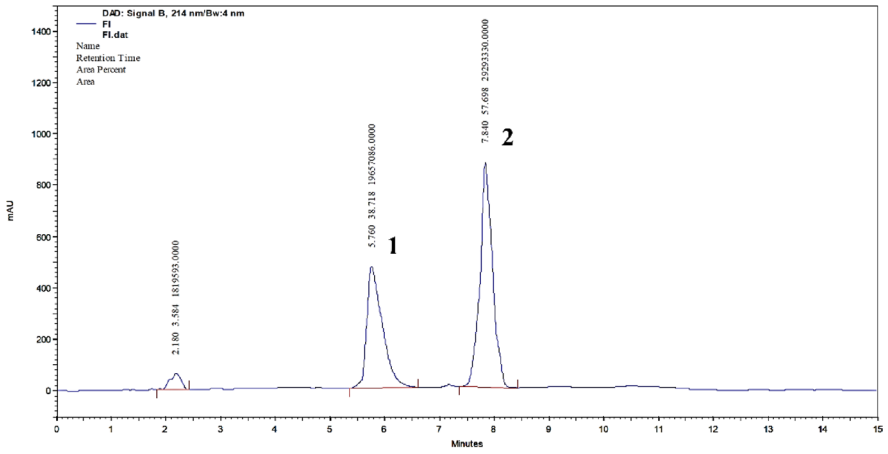

DAD: Signal B,
214 nm/Bw:4 nm
Results

Retention Time	Area	Area %	Height	Height %
2.180	1819593	3.58	129577	4.37
5.760	19657086	38.72	996557	33.62
7.840	29293330	57.70	1838366	62.01
Totals	50770009	100.00	2964500	100.00

B)

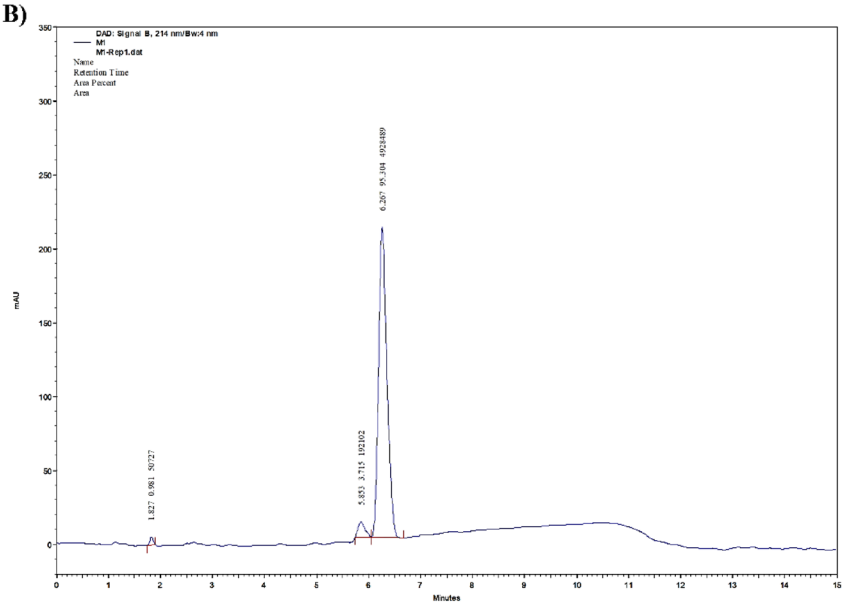

DAD: Signal B,
214 nm/Bw:4 nm
Results

Retention Time	Area	Area %	Height	Height %
1.827	50727	0.98	12035	2.54
5.853	192102	3.71	21331	4.51
6.267	4928489	95.30	440019	92.95
Totals	5171318	100.00	473385	100.00

Fig. 2. Purity chromatogram of L-06 and L-37 by HPLC UV/vis. (**A**) L-06 chromatogram indicating two peaks that subsequently were separated. (**B**) L-37 chromatogram. All the areas under the curve (AUC) percentages for each peak were integrated for calculation of the total purity percentage.

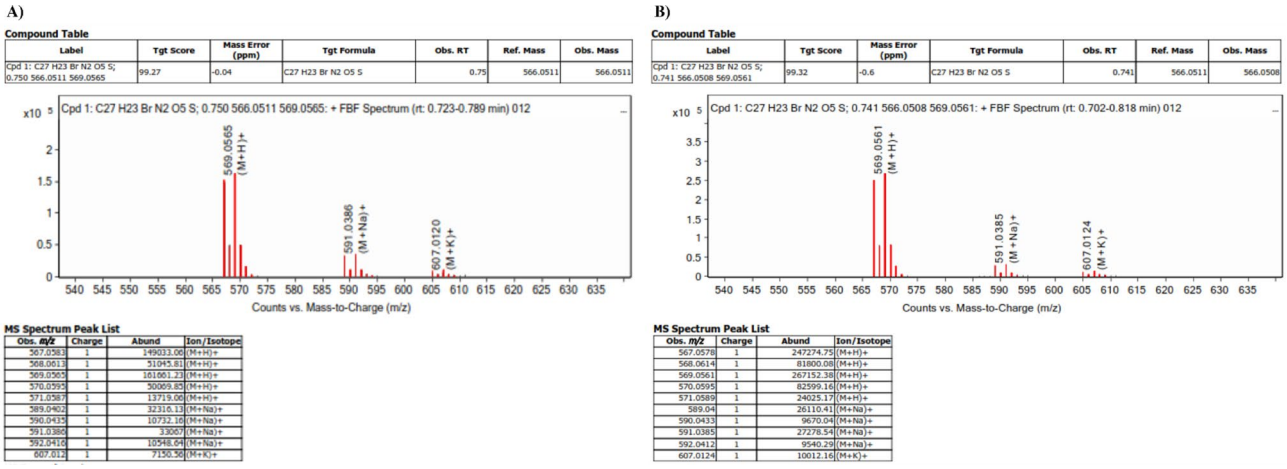

Fig. 3. HPCL-MS/MS chromatograms of the separated peaks of L-06. (**A**) Chromatogram of peak 1 and (**B**) Chromatogram of peak 2. According to the intensity of each peak, for peak 2 is considered as enantiomeric excess.

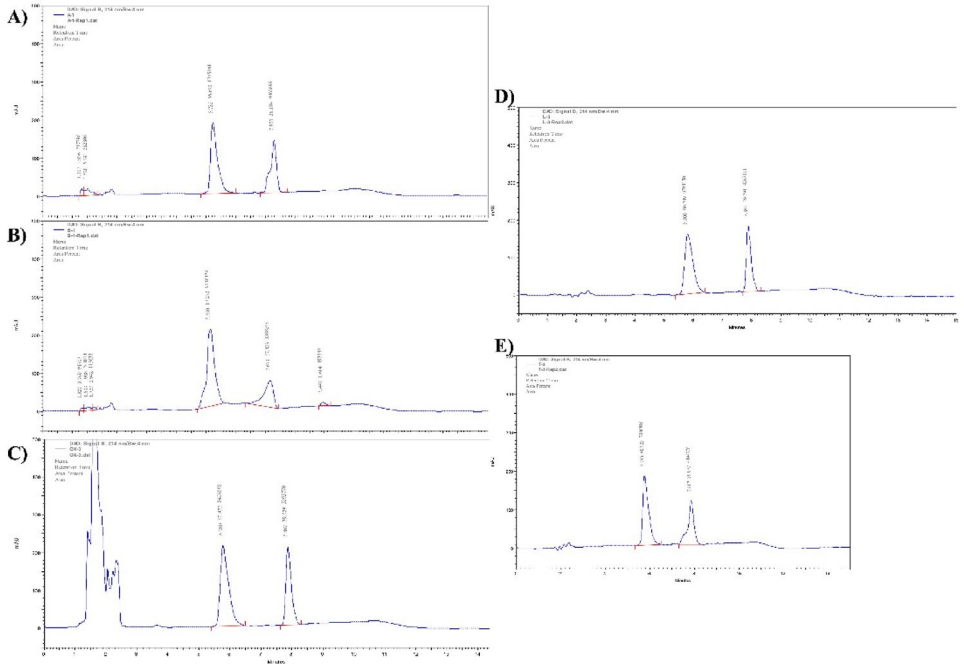

Fig. 4. Chromatograms of L-06 corresponding to Forced Stress assays. (**A**) Acid degradation with 0.1 N HCl condition, (**B**) Basic degradation with 0.1 N NaOH condition, (**C**) Oxidative degradation with 3.0% H_2O_2 condition, (**D**) Luminous degradation with natural light condition and, (**E**) Heat degradation at 50 °C condition.

over classical estrogen receptors α and β) the tested compounds exhibited slightly higher IC_{50} values. However, they demonstrated an increased ability to simultaneously block both pharmacological targets, suggesting a promising dual-inhibition strategy that may reduce the polypharmacology-related side effects commonly associated with first-line therapies for GBM. Nevertheless, the water solubility was improved, considering the inability of G15 to dissolve into medium culture, which formed crystals during the antiproliferative assay at 20 μM, therefore, G15 was not able to reach IC_{50} values in the cells assayed (data not shown). Noteworthy, both cell lines (LN-18 and U373) were more sensitive to L-37 compound than L-06 (Figs. 6 and 7), owing probably to the chlorine atom in the sulfonamide moiety of the ligand which confers a better interaction with the residues forming the binding site for Bcl-2 protein, whose overexpression has been demonstrated elsewhere[35,36]. On the other hand, experimental assays conducted on healthy cells to demonstrate the harmless ability of the synthesized compounds towards no-cancerous cells, showed that both compounds have a higher IC_{50} in human fibroblast cells (BJ) than in the MCF-10 A epithelial cells. Indeed, IC_{50} values obtained for BJ cell line for both

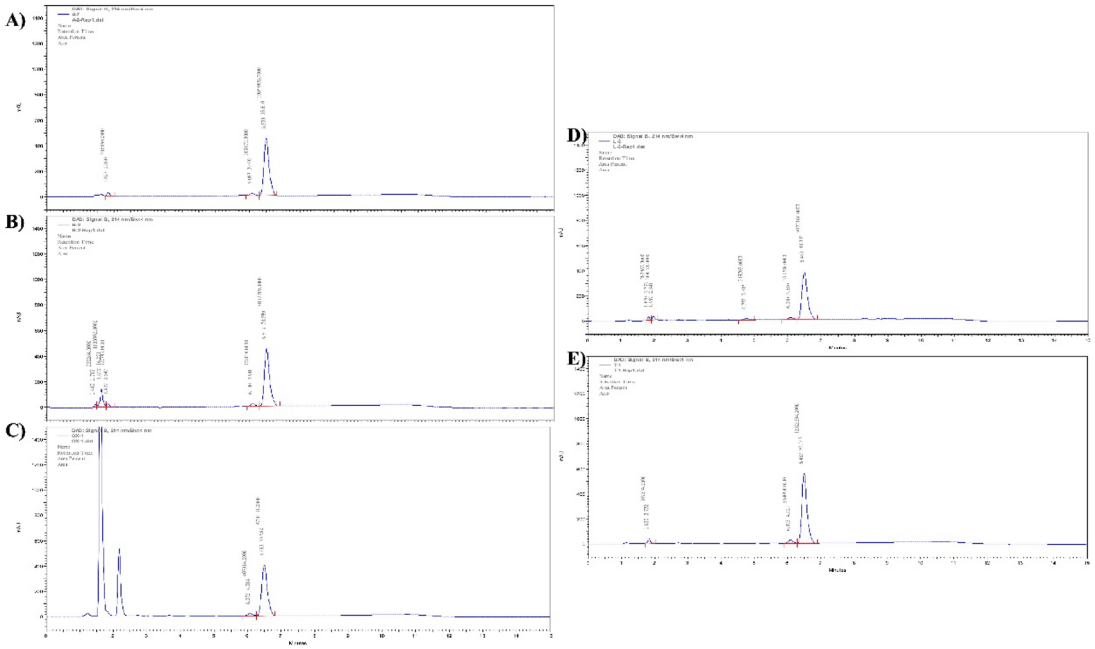

Fig. 5. Chromatograms of L-37 corresponding to Forced Stress assays. (**A**) Acid degradation with 0.1 N HCl condition, (**B**) Basic degradation with 0.1 N NaOH condition, (**C**) Oxidative degradation with 3.0% H_2O_2 condition, (**D**) Luminous degradation with natural light condition and, (**E**) Heat degradation at 50 °C condition.

Compound	Condition				
	Acid	Basic	Oxidative	Luminous	Thermal
L-06	7.2%	9.8%	2.95%	0.15%	1.36%
L-37	0.65%	13.6%	0.5%	3.5%	0.75%

Table 3. Percentage degradation values in each of the assayed conditions of the forced stress assay.

Compounds	IC_{50} (μM)			
	LN-18	U373	BJ	MCF-10 A
L-06	67.66	67.73	102.4	33.78
L-37	40.72	39.78	109.7	23.86
Gossypol	25.26	33.77	N.A.	N.A.

Table 4. IC_{50} values of the assayed compounds on the different cell lines.

compounds were slightly higher than the half of the IC_{50} values reached on the GBM cell lines, whereas, for MCF-10 A the values were strikingly more significant than those reached in both cancer cell lines (Figs. 8 and 9). This can be related to the fact that MCF-10 A has a higher expression of GPER than BJ, as well as the absence of ERα[37]. This difference in expression of the receptor between these two cell lines yields plenty of information about the compound's affinity to GPER. Moreover, the possible interaction of the compounds to GPER may be leading to a probable calcium deregulation in the cell that leads to apoptosis or cell senescence by an additional synergism resulting per se from blocking Bcl-2 activity by the assayed compounds and triggering apoptosis[38–40]. The aforementioned evidence supports the dual-inhibition strategy employed in this study, which targets the aberrant activity of GPER and Bcl-2 in this highly heterogeneous neoplasm. This approach represents a promising alternative to current treatments, which are often limited by high rates of Temozolomide (TMZ) resistance. In contrast, L-06 and L-37 may offer several therapeutic advantages, including the potential to overcome clonal heterogeneity, a reduced risk of MDR, lower drug toxicity, and consequently, fewer side effects. These properties highlight the potential of L-06 and L-37 as effective agents in addressing the challenges posed by this complex and heterogeneous cancer type. Nevertheless, although these results suggest that L-06 and L-37 are cognate ligands of GPER and Bcl-2, further specialized assays are required (such as surface plasmon resonance (SPR), isothermal titration calorimetry (ITC), and high-performance liquid chromatography-mass

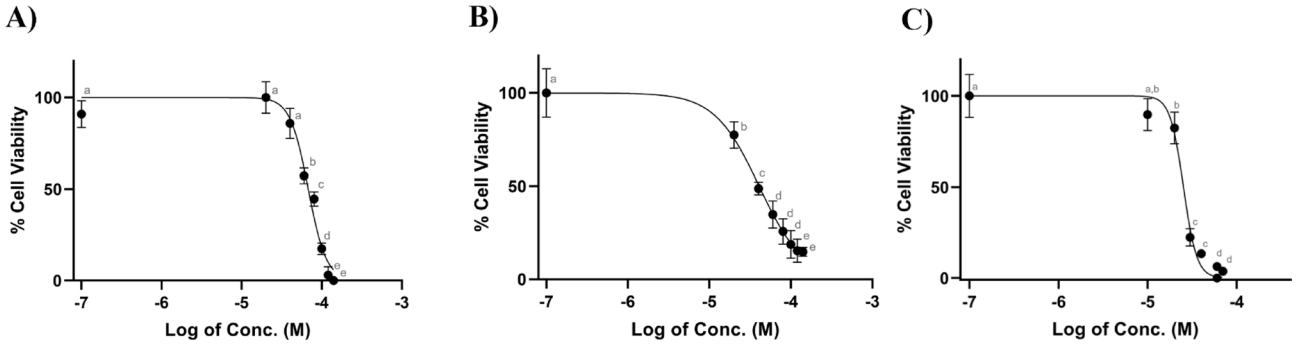

Fig. 6. Concentration-response curve for cell line LN-18 treated with compounds (**A**) L-06, (**B**) L-37 and (**C**) Gossypol. LN-18 cell line was treated with increasing concentrations of the compounds, solubilized in DMSO, ranging from 0 to 140 µM for a duration of 48 h. Cell proliferation was assessed using the MTT assay. Data is presented as mean ± SD ($n = 6$) and has been normalized to 100% relative to the vehicle control for each assay. Statistically significant differences are denoted by different letters ($p < 0.05$).

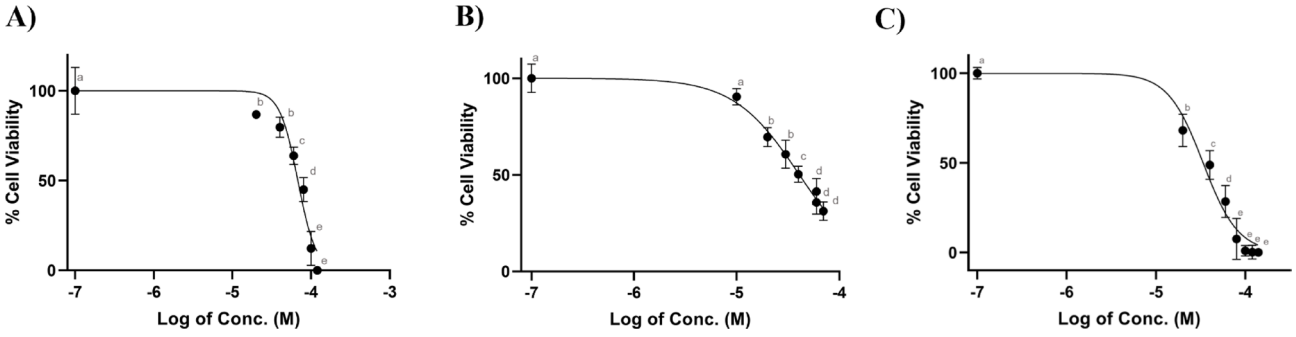

Fig. 7. Concentration-response curve for cell line U373 treated with compounds (**A**) L-06, (**B**) L-37 and (**C**) Gossypol. LN-18 cell line was treated with increasing concentrations of the compounds, solubilized in DMSO, ranging from 0 to 140 µM for a duration of 48 h. Cell proliferation was assessed using the MTT assay. Data is presented as mean ± SD ($n = 6$) and has been normalized to 100% relative to the vehicle control for each assay. Statistically significant differences are denoted by different letters ($p < 0.05$).

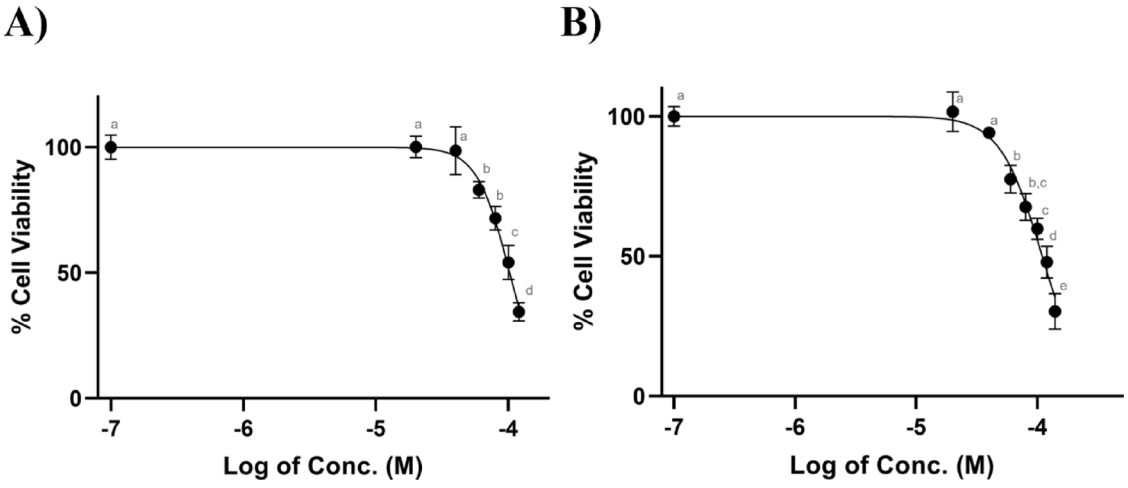

Fig. 8. Concentration-response curve for BJ cell line treated with compounds (**A**) L-06 and (**B**) L-37. BJ cell line was treated with increasing concentrations of the compounds, solubilized in DMSO, ranging from 0 to 140 µM for a duration of 48 h. Cell proliferation was assessed using the MTT assay. Data is presented as mean ± SD ($n = 6$) and has been normalized to 100% relative to the vehicle control for each assay. Statistically significant differences are denoted by different letters ($p < 0.05$).

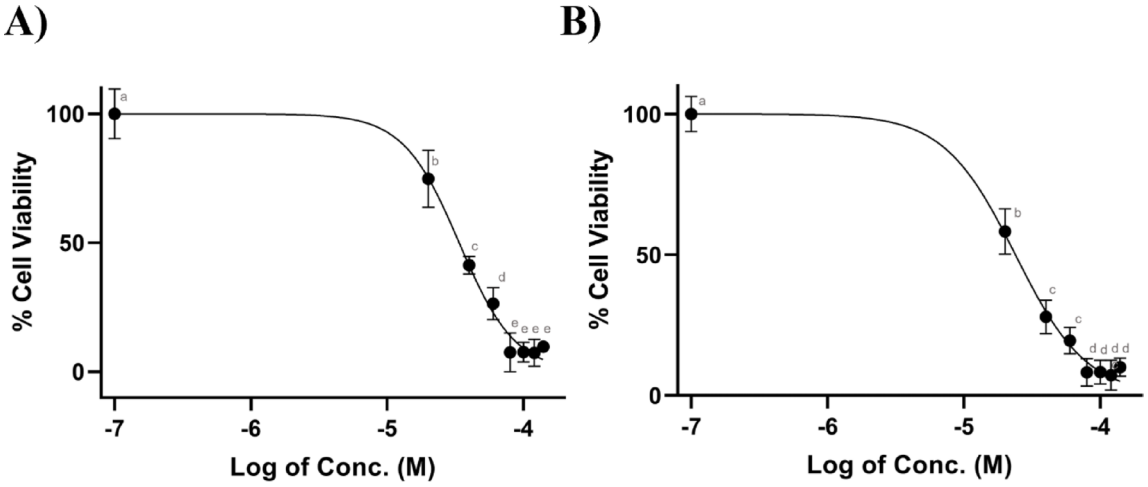

Fig. 9. Concentration-response curve for MCF-10 A cell line treated with compounds (**A**) L-06 and (**B**) L-37. MCF-10 A cell line was treated with increasing concentrations of the compounds, solubilized in DMSO, ranging from 0 to 140 µM for a duration of 48 h. Cell proliferation was assessed using the MTT assay. Data is presented as mean ± SD ($n = 6$) and has been normalized to 100% relative to the vehicle control for each assay. Statistically significant differences are denoted by different letters ($p < 0.05$).

spectrometry (HPLC-MS)) to conclusively determine the affinity of these compounds for the pharmacological targets evaluated in this study. However, G protein–coupled receptors (GPCRs) and intrinsically disordered proteins like Bcl-2 continue to pose significant challenges in the field of protein crystallization[41–43]. Overcoming these challenges will be crucial for the next stage of assays aimed at evaluating the efficacy of the synthesized compounds against glioblastoma multiforme.

L-37 is a better tumor penetrating compound than L-06 against glioblastoma stem cells

Due to their stem-like characteristics, Gli4 cells are capable of growing as neurospheres (NS), consisting of tightly associated clusters of at least several dozen cells. This cell line exhibits high expression of stem cell markers such as CD133+, CD15+, nestin, Sox2, and Olig2. Moreover, Gli4 cells retain the ability to form neurospheres in vitro under appropriate culture conditions, as previously described for both differentiation and proliferation media. Based on these properties, we conducted antiproliferative assays using two distinct cell culture approaches. Specifically, these stem cell markers inherent to Gli4 cells are considered to represent, like other GBM stem cells, highly relevant cellular models to study human brain tumor initiating cells. Therefore, MTT assay results from the flat bottom plates cultured with differentiation medium, shown values in accordance with those yielded from 2D cell cultures assays, in this way, it is evident that both compounds slightly decreased cell viability of the NS compared to G-15, a poorly solubilized GPER antagonist (Fig. 10). This is suggestive of both compounds reaching the binding site described for GPER at lesser degree than G15 deregulating the pathway activated by this receptor, which is involved in cancer progression, invasiveness and migration processes on GBM[60]. Strikingly, NS cultured in proliferation media, which is used to study tumor-penetrating activity of a potential anti-GBM compound, provides valuable information about the ability of L-37 to mimic the behavior of a drug capable of penetrating tumors of central nervous system origin. This is based on their cell anti-proliferation pattern, which shows better performance in round bottom than flat bottom (Fig. 11A and B) correlating with the highly probable ability of this compound to (1) penetrate CNS encapsulated tumors, and (2) avoid tumor size increasing. In detail, NS seeded in round bottom plates were more sensitive to L-37 compounds than L-06 (Fig. 11B), depicting values closely related to the control compound G-15, yielding insights about the key role that GPER leads in promoting tumor formation and growth by GBM stem cells. Altogether, these results point to the ability of the tested compounds (L-37 > L-06) to target and penetrate NS from cancer stem cells with increased anti-cancer treatments resistance, leading to tumor recurrence, progression and non-responsiveness to the current therapies[44–46].

L-37 inhibits the malignant GBM dispersion through neural tissue by 3D cell cultures fixed on nanofibers

A representative hallmark of the most aggressive brain cancers as GBM, is their ability to invade and migrate through neural tissue, driving the failure of the traditional therapies. Thus, an assay conducted with dissociated NS placed on NFS showed the ability of L-37 to depict a conscious trend to decrease cell proliferation in both cell culture mediums employed (proliferation and differentiation mediums) (Fig. 12A and B, respectively). Concisely, Extracellular Matrix (ECM) modifications occurring commonly in first stages of glioma to GMB such as stiffness increasing, glioma cell morphology and nuclear volume which are involved into promotion of the epithelial to mesenchymal transition (EMT), are linked with GPER and Bcl-2 pathways modulation. The probable inhibition of these pharmacological targets in GBM by this type of new dual inhibitors might alter the activity of the involved molecular drivers of these modifications such as N-glycan branching and its interaction

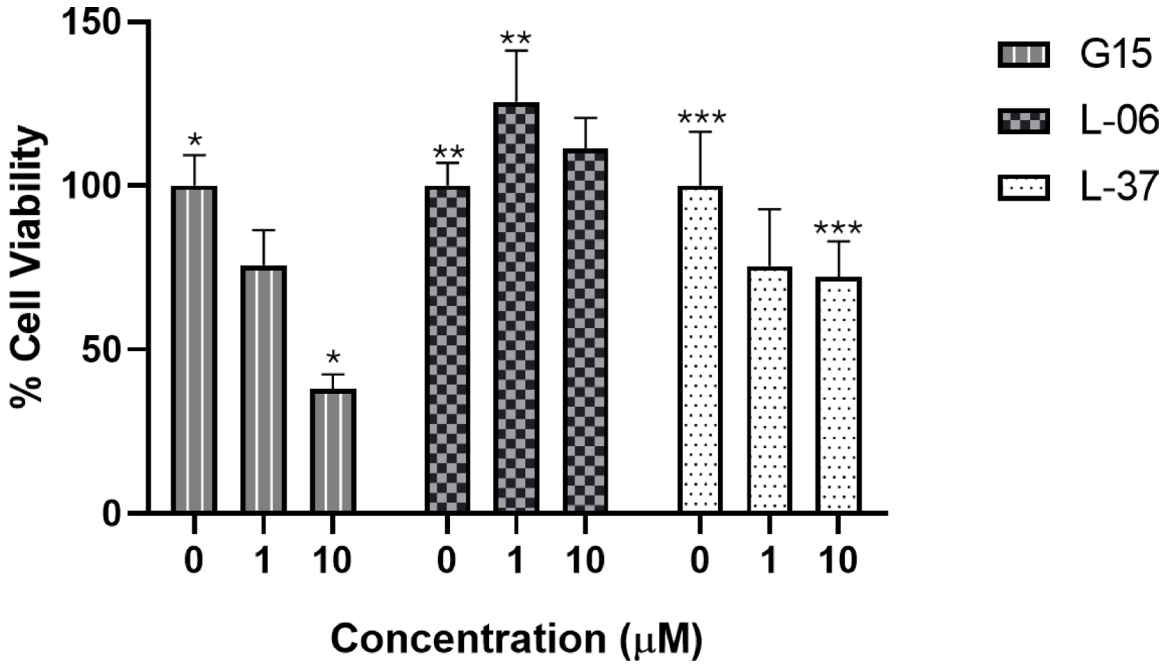

Fig. 10. 4000 cells per well seeded in Differentiation media in a Flat Bottom plate (Treated with Laminin/Lys), MTT assay for quantification 5 days after incubation. $N = 5$ (Y axis is % of viability). Concentration Range: 0, 1 and 10 μM. Statistically significant differences are indicated between treatments by asterisks ($p < 0.05$).

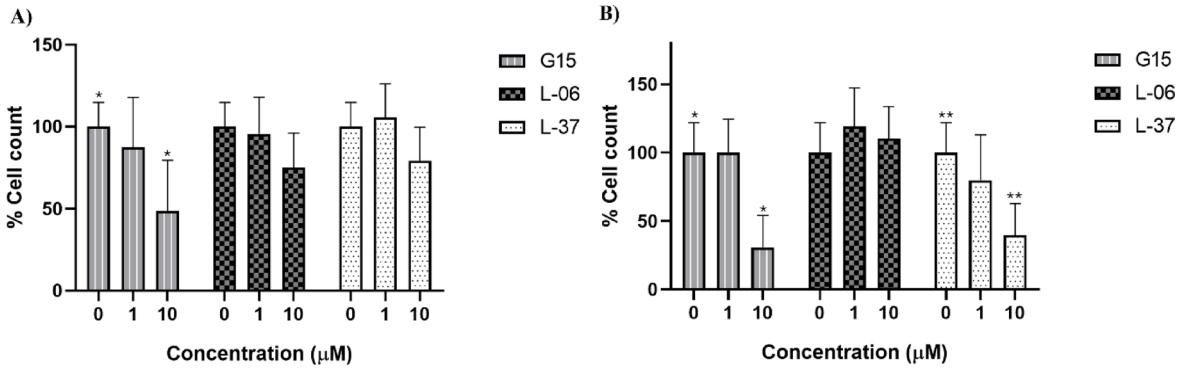

Fig. 11. Neurospheres (NS) 4000 cells per well in proliferation medium, (**A**) Flat Bottom and (**B**) Round Bottom, (Treated with poly-HEMA), cell count 4 days after incubation. $N = 10$ (2 individual experiments) Y axis is % of cell count. Concentration Range: 0, 1 and 10 μM. Statistically significant differences are indicated between treatments by asterisks ($p < 0.05$).

with galectins, or the activity of MGAT5 whose downregulation has been shown to reduce cell migration[47]. Moreover, the interaction between galectin and branched N-glycans on integrins (proteins of the cell surface) have been associated with turnover and maturation of Focal Adhesion (FA), fibronectin fibrillogenesis and actin microfilament remodelling. In that way, it is noteworthy that actin microfilaments have been postulated as other molecular target of compounds including in their structure the tetrahydroquinoline scaffold (as G1 and G15, synthetic ligands of GPER), which might potentiate the anti-migratory effect of the assayed compounds via different molecular mechanisms than the RhoA and the subsequent activation of ROCK and phospho-myosin light chain 2 (pMLC2) founded in other cancer types as pancreatin and prostate which involves the GPER activation[48–50]. Is important to note that Gli4 cells on NFS were more sensitive to L-37 than L-06, with outstanding inhibition values in accordance to depicted by G15 in proliferation medium which is serum-free, supplemented with β-FGF and EGF allowing the propagation of multipotent, self-renewing tumor-spheres (NS)[51], at the three assayed concentrations (0.1, 1, and 10 μM), denoting the pivotal role of GPER into promoting the migration mechanism of glioblastomas stem-like cells (GSCs). Furthermore, it is worth mentioning that the non-antiproliferative activity of L-06 depicts an interesting behavior which tends to show discreet cell proliferation, may be due to a poly pharmacology effect in which the compound interacts with different macromolecules than GPER, leading to an apparent resistance to the cell treatment (Fig. 12A and B).

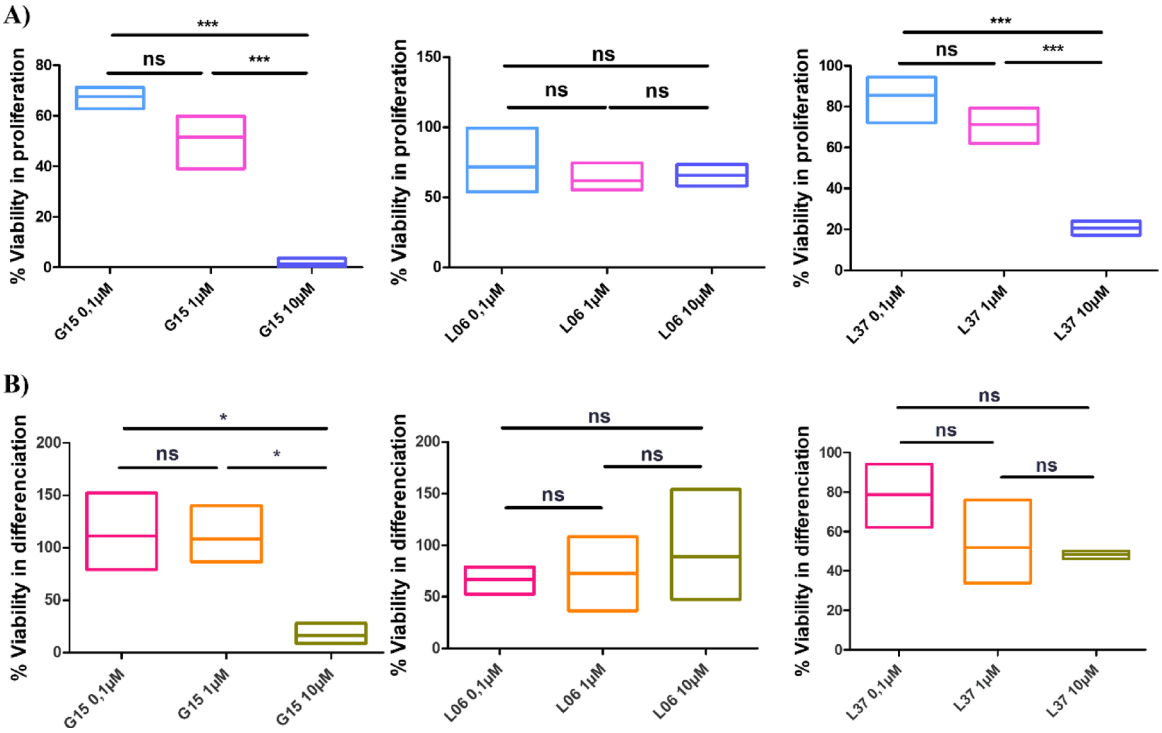

Fig. 12. Gli4 cells on non-aligned nanofibers, 4000 cells per well, (**A**) in Proliferation medium and (**B**) Differentiation medium, 4000 cells per well, with cell counting performed 4 days after incubation. $n = 3$ (individual experiments). The Y-axis represents the percentage of cell viability. Concentration range: 0.1, 1, and 10 µM.

Cell migration is inhibited in a concentration-response fashion at non-cytotoxic concentrations range

It is well-known the key role that GPER triggers into preserving cell migration and invasiveness as has been described for cancer cell lines[52,53] different to GMB. In this sense, for astrocyte enriched culture and astrocyte-derived C6 clonal cells, GPER activates PI3K/FAK/Akt/RhoA/Rac1/Cdc42 signaling pathway, resulting in increased glial cell migration[54,55]. To analyze these premises, we conducted cell migration inhibitory assays in which the concentrations used to inhibit migration varied between compounds, as we specifically selected concentrations that did not exhibit cytotoxic effects. The goal was to observe the inhibition of cell migration independently of any cytotoxic effects on proliferating cells. This means that migration inhibition occurs within a concentration range that does not induce cytotoxicity (Fig. 13). In these conditions L-06 assayed at 10 µM but not G-15 nor L-37 at 2 µM, reduces by nearly 50% the migration of Gli4 cells on aligned NFS (Fig. 13A). Furthermore, G-15 and L-37 assayed at concentrations in which an antiproliferative effect was observed previously, we note a discreet antimigratory effect (data not shown) but, under this condition, it is difficult to attribute it to a strictly their antiproliferative ability performed in other assays herein conducted. These findings underscore the substantial therapeutic potential of L-06 to a greater extent than G-15 and L-37 compounds, to inhibit GPER and Bcl-2, by targeting cell migration, an essential factor in the progression, invasiveness, and poor prognosis of GBM. Regarding the molecular mechanisms underlying the inhibition of cell migration, it is highly likely that this occurs through a synergistic effect. This effect is mediated by the blockade of Bcl-2, which leads to the inhibition of Furin activity and several matrix metalloproteinases (MMPs), including MT1-MMP, MMP-2/-9[56,57]. Additionally, the inhibition of GPER activity further contributes to this synergism. In that sense, it is worth noting that a molecular mediator from the GPER pathway is the activation of EGFR which results from the transactivation mediated by the β/γ subunit of the G-protein coupled to the receptor, therefore blocking of the GPER activity on Gli4 cells leads to an efficient antimigratory effect instaured up-stream on the pathway triggered for the receptor (Fig. 13A and B), as has been analyzed for selective EGFR inhibitors[58,59].

LN-18 and U373 are suitable cell models of GPER expression

Western blot analysis for GPER expression in LN-18 and U373 cell lines revealed an unexpected 25 kDa band, contrary to the anticipated 42 kDa molecular weight of GPER. However, according elsewhere, GPER has been identified at 70 and 55 kDa associated with receptor maturation through N-glycosylation, moreover, diverse isoforms of GPER with weights spanning from 40 to 110 kDa have been detected[60]. Additionally, GPER expression in brain tissue, as evidenced by western blot, displayed a distinct 25 kDa band, noticeably absent in vascular smooth muscle cells subjected to identical receptor identification[61]. Interestingly, this difference suggests a potential metabolic divergence in GPER expression between brain tissue and peripheral regions. Another plausible explanation may lie in the likelihood of GPER undergoing protein cleavage or degradation processes,

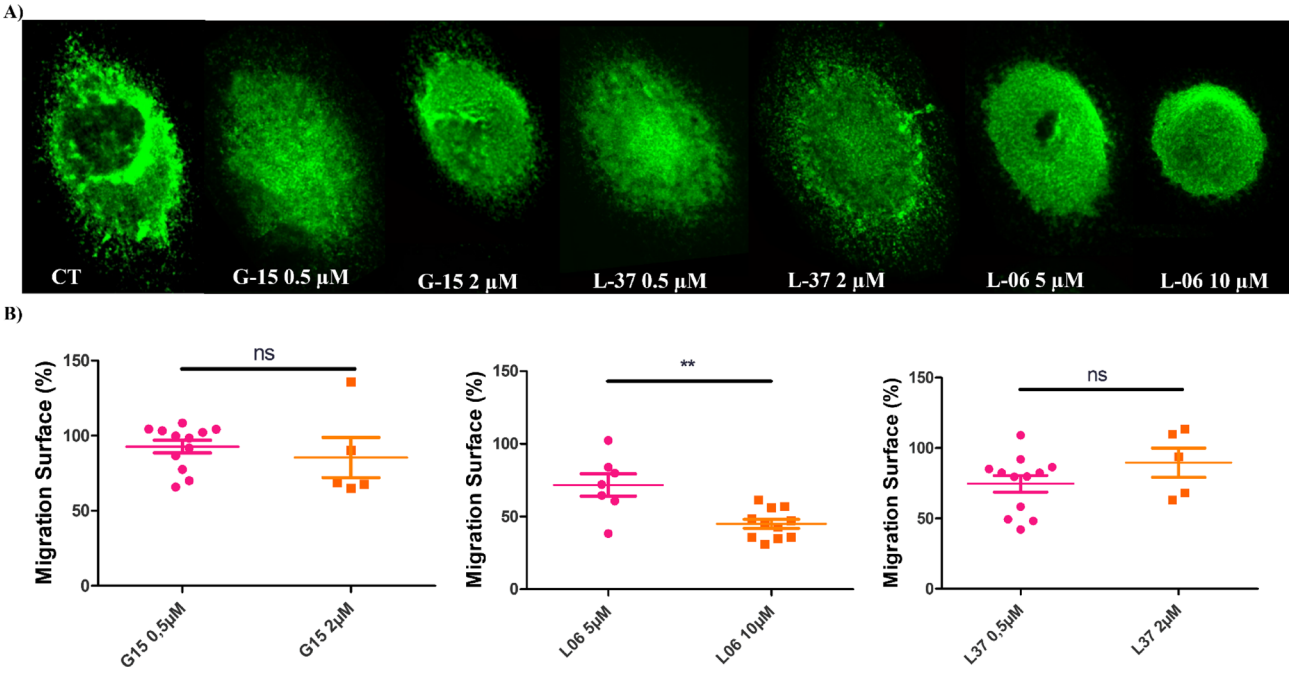

Fig. 13. Migration of Gli4 cells. Neurospheres containing 5000 cells were deposited on aligned fibers in proliferation medium. (**A**) Migration area measurements were performed 5 days after neurospheres deposition. (**B**) Migration surface %. The Y-axis represents the surface area in µm². Concentration range: 0 µM for control (Ctrl), 0.5 and 2 µM for G15 and L-37; and 5 and 10 µM for L-37.

contributing to the observed molecular weight disparity in GPER expression within LN-18 and U373 cell lines (Fig. 14). This phenomenon has been previously reported for GPER expression in several GPER-transfected cell lines, including HeLa, HEK, and MDCK, where a lower band ranging between 20 and 30 kDa was observed, likely representing degradation products. Additionally, it is highly probable that both N-glycosylation and degradation processes are occurring in LN-18 and U373 cell lines, potentially due to the influence of the cancer microenvironment. This may explain the appearance of the unexpected 25 kDa band, as reported elsewhere[62]. For further information about WB gel see Fig. S1 in Supplementary Material.

Conclusion

A crucial step into new drug development is to demonstrate all the assays encompassed in preclinical pharmacology, aimed to address cost and human issues directly related to a novel drug either through in vitro and in vivo evaluations. Thus, in this work we showed the results yielded by a battery of in vitro assays that depicts the potential anti glioblastoma activity of two new compounds focused towards GPER and Bcl-2 pharmacological targets. Specifically, the purity analysis from HPLC UV/Vis showed the safety and harmlessness of L-06 and L-37 compounds, which, even submitted to forced degradation assays under several medium conditions, maintain a suitable integrity percentage establishing the basis for consequent pharmaceutics evaluations for the search of a pharmaceutical formulation. In addition, antiproliferative analysis in classic 2D cell culture conditions yield plenty of information about the ability of L-06 and L-37 to decrease cell proliferation of LN-18 and U373 GBM cell lines with IC_{50} values closely related to the obtained values for Gossypol (a Bcl-2 inhibitor), with a slightly better performance of L-37 than L-06. Besides, as result of 3D cell cultures applying two approaches, NS formation on specific cell culture medium conditions and, dissociated glioblastoma stem cells loaded on NFS we analyzed their antiproliferative activity on a tumor-like environment of the synthesized compounds. Moreover, we were able to analyze that Gli4 NS formation was especially sensitive to L-37 compound whose IC_{50} values were in correlation to those obtained for G-15, while, dissociated Gli4 loaded on NFS only L-37 yielded the most promissory results to inhibiting the cell viability at almost equal values than G15 ligand in both cell medium conditions (differentiation and proliferation). Furthermore, results from the anti-migratory assays point out to a synergistic anti migratory effect resulting from a GPER and Bcl-2 inhibition at non-cytotoxic concentrations. Lastly, we were able to analyze the GPER expression on the cell models employed for the 2D antiproliferative assays. Evidently, further specific assays that are currently in development are required to fully elucidate the molecular mechanisms modulated by the tested ligands through these pharmacological targets. For GPER activity, assays such as Ca^{2+} mobilization and/or cAMP production measurements should be conducted, while Bcl-2 activity can be assessed using FRET or competition pull-down assays, all of them in in vitro models. Additionally, further preclinical research involving more complex assays, such as testing in in vivo models like the murine GBM model and evaluating the local administration of the synthesized compounds via intracerebroventricular injection (ICV), will provide valuable insights into the anti-glioblastoma properties of the tested compounds. In this context, SPR, ITC, and HPLC-MS assays will be essential to determine the

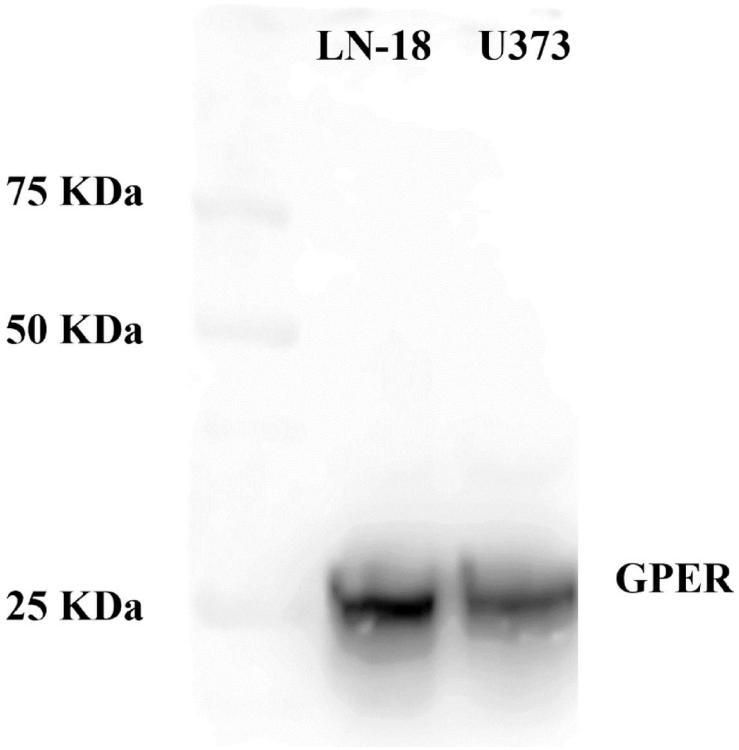

Fig. 14. Expression of GPER in LN-28 and U373 cell lines with a MW of ~ 25 kDa. The image was adjusted by increasing its contrast solely to enhance visualization.

binding affinities of the synthesized compounds to GPER and Bcl-2. However, crystallization of these proteins in complex with diffusible ligands remains a significant challenge. Key obstacles include the poor solubility of ligand–receptor complexes, limited understanding of protein dynamics and conformational heterogeneity, and the difficulty in detecting post-translational modifications. Overcoming these challenges will be crucial for the next phase of our research, which is focused on the development of effective anti-glioblastoma compounds. Nevertheless, all the data presented above places L-06 and L-37 as two potential candidates to employ as anti-glioblastoma therapy.

Data availability

The datasets used and/or analysed during the current study available from the corresponding author on reasonable request.

Received: 20 December 2024; Accepted: 12 May 2025
Published online: 21 May 2025

5. References

1. Prager, B. C., Bhargava, S., Mahadev, V., Hubert, C. G. & Rich, J. N. Glioblastoma stem cells: driving resilience through Chaos. *Trends Cancer*. **6**, 223–235. https://doi.org/10.1016/j.trecan.2020.01.009 (2020).
2. Stupp, R., Tonn, J. C., Brada, M., Pentheroudakis, G. & Group, E. G. W. High-grade malignant glioma: ESMO clinical practice guidelines for diagnosis, treatment and follow-up. *Ann. Oncol.* **21** (Suppl 5), v190–193. https://doi.org/10.1093/annonc/mdq187 (2010).
3. Angom, R. S., Nakka, N. M. R. & Bhattacharya, S. Advances in glioblastoma therapy: an update on current approaches. *Brain Sci.* **13** https://doi.org/10.3390/brainsci13111536 (2023).
4. Wu, W. et al. Glioblastoma multiforme (GBM): an overview of current therapies and mechanisms of resistance. *Pharmacol. Res.* **171**, 105780. https://doi.org/10.1016/j.phrs.2021.105780 (2021).
5. Rong, L., Li, N. & Zhang, Z. Emerging therapies for glioblastoma: current state and future directions. *J. Exp. Clin. Cancer Res.* **41**, 142. https://doi.org/10.1186/s13046-022-02349-7 (2022).
6. Zhu, P., Du, X. L., Lu, G. & Zhu, J. J. Survival benefit of glioblastoma patients after FDA approval of Temozolomide concomitant with radiation and bevacizumab: A population-based study. *Oncotarget* **8**, 44015–44031. https://doi.org/10.18632/oncotarget.17054 (2017).
7. Stupp, R. et al. Radiotherapy plus concomitant and adjuvant Temozolomide for glioblastoma. *N Engl. J. Med.* **352**, 987–996. https://doi.org/10.1056/NEJMoa043330 (2005).
8. Holland, E. C. Glioblastoma multiforme: the terminator. *Proc. Natl. Acad. Sci. U S A*. **97**, 6242–6244. https://doi.org/10.1073/pnas.97.12.6242 (2000).
9. Lee, S. Y. Temozolomide resistance in glioblastoma multiforme. *Genes Dis.* **3**, 198–210. https://doi.org/10.1016/j.gendis.2016.04.007 (2016).

10. Teraiya, M., Perreault, H. & Chen, V. C. An overview of glioblastoma multiforme and Temozolomide resistance: can LC-MS-based proteomics reveal the fundamental mechanism of Temozolomide resistance? *Front. Oncol.* **13**, 1166207. https://doi.org/10.3389/fonc.2023.1166207 (2023).
11. Hegi, M. E. et al. MGMT gene Silencing and benefit from Temozolomide in glioblastoma. *N Engl. J. Med.* **352**, 997–1003. https://doi.org/10.1056/NEJMoa043331 (2005).
12. Zhao, H., Wang, S., Song, C., Zha, Y. & Li, L. The prognostic value of MGMT promoter status by pyrosequencing assay for glioblastoma patients' survival: a meta-analysis. *World J. Surg. Oncol.* **14**, 261. https://doi.org/10.1186/s12957-016-1012-4 (2016).
13. Weller, M. et al. MGMT promoter methylation in malignant gliomas: ready for personalized medicine? *Nat. Rev. Neurol.* **6**, 39–51. https://doi.org/10.1038/nrneurol.2009.197 (2010).
14. Taylor, O. G., Brzozowski, J. S. & Skelding, K. A. Glioblastoma multiforme: an overview of emerging therapeutic targets. *Front. Oncol.* **9**, 963. https://doi.org/10.3389/fonc.2019.00963 (2019).
15. Cancer Genome Atlas Research, N. Comprehensive genomic characterization defines human glioblastoma genes and core pathways. *Nature* **455**, 1061–1068. https://doi.org/10.1038/nature07385 (2008).
16. Zhang, Y. et al. Inhibition of Bcl-2/Bcl-xL and c-MET causes synthetic lethality in model systems of glioblastoma. *Sci. Rep.* **8**, 7373. https://doi.org/10.1038/s41598-018-25802-0 (2018).
17. Antonietti, P. et al. Interference with the HSF1/HSP70/BAG3 pathway primes glioma cells to matrix detachment and BH3 Mimetic-Induced apoptosis. *Mol. Cancer Ther.* **16**, 156–168. https://doi.org/10.1158/1535-7163.MCT-16-0262 (2017).
18. Adams, J. M. & Cory, S. The BCL-2 arbiters of apoptosis and their growing role as cancer targets. *Cell. Death Differ.* **25**, 27–36. https://doi.org/10.1038/cdd.2017.161 (2018).
19. Yague, J. G., Lavaque, E., Carretero, J., Azcoitia, I. & Garcia-Segura, L. M. Aromatase, the enzyme responsible for Estrogen biosynthesis, is expressed by human and rat glioblastomas. *Neurosci. Lett.* **368**, 279–284. https://doi.org/10.1016/j.neulet.2004.07.010 (2004).
20. Duenas Jimenez, J. M. et al. Aromatase and Estrogen receptor alpha mRNA expression as prognostic biomarkers in patients with Astrocytomas. *J. Neurooncol.* **119**, 275–284. https://doi.org/10.1007/s11060-014-1509-z (2014).
21. Hsu, L. H., Chu, N. M., Lin, Y. F. & Kao, S. H. G-Protein coupled Estrogen receptor in breast Cancer. *Int. J. Mol. Sci.* **20** https://doi.org/10.3390/ijms20020306 (2019).
22. Filardo, E. J., Quinn, J. A., Bland, K. I. & Frackelton, A. R. Jr. Estrogen-induced activation of Erk-1 and Erk-2 requires the G protein-coupled receptor homolog, GPR30, and occurs via trans-activation of the epidermal growth factor receptor through release of HB-EGF. *Mol. Endocrinol.* **14**, 1649–1660. https://doi.org/10.1210/mend.14.10.0532 (2000).
23. Shi, D. et al. Inhibition of PI3K/AKT molecular pathway mediated by membrane Estrogen receptor GPER accounts for Cryptotanshinone induced antiproliferative effect on breast cancer SKBR-3 cells. *BMC Pharmacol. Toxicol.* **21**, 32. https://doi.org/10.1186/s40360-020-00410-9 (2020).
24. Wang, Y. & Tortorella, M. Molecular design of dual inhibitors of PI3K and potential molecular target of cancer for its treatment: A review. *Eur. J. Med. Chem.* **228**, 114039. https://doi.org/10.1016/j.ejmech.2021.114039 (2022).
25. Zhou, J. et al. Rational design of Multitarget-Directed ligands: strategies and emerging paradigms. *J. Med. Chem.* **62**, 8881–8914. https://doi.org/10.1021/acs.jmedchem.9b00017 (2019).
26. Zhang, D. et al. Current progress and prospects for G protein-coupled Estrogen receptor in triple-negative breast cancer. *Front. Cell. Dev. Biol.* **12**, 1338448. https://doi.org/10.3389/fcell.2024.1338448 (2024).
27. Yu, T. et al. GPER mediates enhanced cell viability and motility via non-genomic signaling induced by 17beta-estradiol in triple-negative breast cancer cells. *J. Steroid Biochem. Mol. Biol.* **143**, 392–403. https://doi.org/10.1016/j.jsbmb.2014.05.003 (2014).
28. Morelos-Garnica, L. A. et al. In Silico design and cell-based evaluation of two dual anti breast cancer compounds targeting Bcl-2 and GPER. *Sci. Rep.* **13**, 17933. https://doi.org/10.1038/s41598-023-43860-x (2023).
29. Ortiz-Morales, A. A. et al. PAMAM-G4 protect the N-(2-hydroxyphenyl)-2-propylpentanamide (HO-AAVPA) and maintain its antiproliferative effects on MCF-7. *Sci. Rep.* **13**, 3383. https://doi.org/10.1038/s41598-023-30144-7 (2023).
30. Guichet, P. O. et al. Cell death and neuronal differentiation of glioblastoma stem-like cells induced by neurogenic transcription factors. *Glia* **61**, 225–239. https://doi.org/10.1002/glia.22429 (2013).
31. Saleh, A. et al. A novel 3D nanofibre scaffold conserves the plasticity of glioblastoma stem cell invasion by regulating galectin-3 and integrin-beta1 expression. *Sci. Rep.* **9**, 14612. https://doi.org/10.1038/s41598-019-51108-w (2019).
32. Kmecz, I. et al. Optical resolution of 6-fluoro-2-methyl-1,2,3,4-tetrahydroquinoline by supercritical fluid extraction. *Chirality* **13**, 568–570. https://doi.org/10.1002/chir.1178 (2001).
33. Santos, S. D. et al. PAMAM dendrimers: blood-brain barrier transport and neuronal uptake after focal brain ischemia. *J. Control Release.* **291**, 65–79. https://doi.org/10.1016/j.jconrel.2018.10.006 (2018).
34. Flores-Mejia, R. et al. Chemical characterization (LC-MS-ESI), cytotoxic activity and intracellular localization of PAMAM G4 in leukemia cells. *Sci. Rep.* **11**, 8210. https://doi.org/10.1038/s41598-021-87560-w (2021).
35. Zhang, C. et al. Mechanisms involved in the anti-tumor effects of Toosendanin in glioma cells. *Cancer Cell. Int.* **21**, 492. https://doi.org/10.1186/s12935-021-02186-2 (2021).
36. Sesen, J. et al. Int6/eIF3e is essential for proliferation and survival of human glioblastoma cells. *Int. J. Mol. Sci.* **15**, 2172–2190. https://doi.org/10.3390/ijms15022172 (2014).
37. Deng, Y., Miki, Y. & Nakanishi, A. Estradiol/GPER affects the integrity of mammary duct-like structures in vitro. *Sci. Rep.* **10**, 1386. https://doi.org/10.1038/s41598-020-57819-9 (2020).
38. Morris, J. L., Gillet, G., Prudent, J. & Popgeorgiev, N. Bcl-2 family of proteins in the control of mitochondrial calcium signalling: an old chap with new roles. *Int. J. Mol. Sci.* **22** https://doi.org/10.3390/ijms22073730 (2021).
39. Chiu, W. T. et al. Bcl(-)2 regulates store-operated Ca(2+) entry to modulate ER stress-induced apoptosis. *Cell. Death Discov.* **4**, 37. https://doi.org/10.1038/s41420-018-0039-4 (2018).
40. Callens, M. et al. The role of Bcl-2 proteins in modulating neuronal Ca(2+) signaling in health and in Alzheimer's disease. *Biochim. Biophys. Acta Mol. Cell. Res.* **1868**, 118997. https://doi.org/10.1016/j.bbamcr.2021.118997 (2021).
41. Dijkman, P. M. et al. Conformational dynamics of a G protein-coupled receptor helix 8 in lipid membranes. *Sci. Adv.* **6**, eaav8207. https://doi.org/10.1126/sciadv.aav8207 (2020).
42. Zhao, Q. & Wu, B. L. Ice breaking in GPCR structural biology. *Acta Pharmacol. Sin.* **33**, 324–334. https://doi.org/10.1038/aps.2011.187 (2012).
43. Zhang, M. et al. G protein-coupled receptors (GPCRs): advances in structures, mechanisms, and drug discovery. *Signal. Transduct. Target. Ther.* **9**, 88. https://doi.org/10.1038/s41392-024-01803-6 (2024).
44. Hambardzumyan, D., Squatrito, M., Carbajal, E. & Holland, E. C. Glioma formation, cancer stem cells, and Akt signaling. *Stem Cell. Rev.* **4**, 203–210. https://doi.org/10.1007/s12015-008-9021-5 (2008).
45. Lathia, J. D. et al. Direct in vivo evidence for tumor propagation by glioblastoma cancer stem cells. *PLoS One.* **6**, e24807. https://doi.org/10.1371/journal.pone.0024807 (2011).
46. P, C. J. et al. In vitro neurosphere formation correlates with poor survival in glioma. *IUBMB Life.* **71**, 244–253. https://doi.org/10.1002/iub.1964 (2019).
47. Guo, H. et al. Transcriptional regulation of the Protocadherin beta cluster during Her-2 protein-induced mammary tumorigenesis results from altered N-glycan branching. *J. Biol. Chem.* **287**, 24941–24954. https://doi.org/10.1074/jbc.M112.369355 (2012).
48. Rice, A. et al. GPER activation inhibits Cancer cell mechanotransduction and basement membrane invasion via RhoA. *Cancers (Basel).* **12** https://doi.org/10.3390/cancers12020289 (2020).

49. Masi, M., Racchi, M., Travelli, C., Corsini, E. & Buoso, E. Molecular characterization of membrane steroid receptors in Hormone-Sensitive cancers. *Cells* **10** https://doi.org/10.3390/cells10112999 (2021).
50. Friedl, P. & Gilmour, D. Collective cell migration in morphogenesis, regeneration and cancer. *Nat. Rev. Mol. Cell. Biol.* **10**, 445–457. https://doi.org/10.1038/nrm2720 (2009).
51. Marhuenda, E. et al. Glioma stem cells invasive phenotype at optimal stiffness is driven by MGAT5 dependent mechanosensing. *J. Exp. Clin. Cancer Res.* **40**, 139. https://doi.org/10.1186/s13046-021-01925-7 (2021).
52. Yang, H., Wang, C., Liao, H. & Wang, Q. Activation of GPER by E2 promotes proliferation, invasion and migration of breast cancer cells by regulating the miR-124/CD151 pathway. *Oncol. Lett.* **21**, 432. https://doi.org/10.3892/ol.2021.12693 (2021).
53. Yan, Y., Jiang, X., Zhao, Y., Wen, H. & Liu, G. Role of GPER on proliferation, migration and invasion in ligand-independent manner in human ovarian cancer cell line SKOV3. *Cell. Biochem. Funct.* **33**, 552–559. https://doi.org/10.1002/cbf.3154 (2015).
54. Ariyani, W., Miyazaki, W. & Koibuchi, N. A. Novel mechanism of S-equol action in neurons and astrocytes: the possible involvement of GPR30/GPER1. *Int. J. Mol. Sci.* **20** https://doi.org/10.3390/ijms20205178 (2019).
55. Ariyani, W. et al. Soy isoflavones accelerate glial cell migration via GPER-Mediated signal transduction pathway. *Front. Endocrinol. (Lausanne)*. **11**, 554941. https://doi.org/10.3389/fendo.2020.554941 (2020).
56. Wick, W., Wild-Bode, C., Frank, B. & Weller, M. BCL-2-induced glioma cell invasiveness depends on furin-like proteases. *J. Neurochem*. **91**, 1275–1283. https://doi.org/10.1111/j.1471-4159.2004.02806.x (2004).
57. Um, H. D. Bcl-2 family proteins as regulators of cancer cell invasion and metastasis: a review focusing on mitochondrial respiration and reactive oxygen species. *Oncotarget* **7**, 5193–5203. https://doi.org/10.18632/oncotarget.6405 (2016).
58. Parker, J. J. et al. Gefitinib selectively inhibits tumor cell migration in EGFR-amplified human glioblastoma. *Neuro Oncol.* **15**, 1048–1057. https://doi.org/10.1093/neuonc/not053 (2013).
59. Westphal, M., Maire, C. L. & Lamszus, K. EGFR as a target for glioblastoma treatment: an unfulfilled promise. *CNS Drugs*. **31**, 723–735. https://doi.org/10.1007/s40263-017-0456-6 (2017).
60. Pena-Gutierrez, K. M., Hernandez-Ortega, K. & Bello-Alvarez, C. Camacho-Arroyo, I. Expression and Estrogen regulation of G protein-coupled Estrogen receptor in human glioblastoma cells. *Oncol. Lett.* **24**, 397. https://doi.org/10.3892/ol.2022.13517 (2022).
61. Zimmerman, M. A., Budish, R. A., Kashyap, S. & Lindsey, S. H. GPER-novel membrane oestrogen receptor. *Clin. Sci. (Lond)*. **130**, 1005–1016. https://doi.org/10.1042/CS20160114 (2016).
62. Sanden, C. et al. G protein-coupled Estrogen receptor 1/G protein-coupled receptor 30 localizes in the plasma membrane and traffics intracellularly on cytokeratin intermediate filaments. *Mol. Pharmacol.* **79**, 400–410. https://doi.org/10.1124/mol.110.069500 (2011).

Acknowledgements

The authors thank the Instituto Politécnico Nacional (SIP), BEIFI, COFAA-EDI-IPN and the National Council of Science and Technology (CONAHCyT) for its grants: CB 254600 and Ecos Nord 296637.

Author contributions

D. M. L. wrote the original draft and conducted the chemical synthesis and related assays. L. A. M. G. and J. R. G. S. performed the 2D culture assays and WB analysis. G. J. and L. B. conducted the 3D culture and antimigratory assays. J. C. B. and N. B. did the funding acquisition and supervised the investigation.

Declarations

Competing interests

The authors declare no competing interests.

Additional information

Supplementary Information The online version contains supplementary material available at https://doi.org/10.1038/s41598-025-02186-6.

Correspondence and requests for materials should be addressed to N.B. or J.C.-B.

Reprints and permissions information is available at www.nature.com/reprints.

Publisher's note Springer Nature remains neutral with regard to jurisdictional claims in published maps and institutional affiliations.

Open Access This article is licensed under a Creative Commons Attribution-NonCommercial-NoDerivatives 4.0 International License, which permits any non-commercial use, sharing, distribution and reproduction in any medium or format, as long as you give appropriate credit to the original author(s) and the source, provide a link to the Creative Commons licence, and indicate if you modified the licensed material. You do not have permission under this licence to share adapted material derived from this article or parts of it. The images or other third party material in this article are included in the article's Creative Commons licence, unless indicated otherwise in a credit line to the material. If material is not included in the article's Creative Commons licence and your intended use is not permitted by statutory regulation or exceeds the permitted use, you will need to obtain permission directly from the copyright holder. To view a copy of this licence, visit http://creativecommons.org/licenses/by-nc-nd/4.0/.

© The Author(s) 2025